Talanta 117 (2013) 70–74

Contents lists available at ScienceDirect

Talanta

journal homepage: www.elsevier.com/locate/talanta

Colorimetric detection of Al^{3+} ions using triazole–ether functionalized gold nanoparticles

Yu-Ching Chen, I-Lin Lee, Yi-Ming Sung, Shu-Pao Wu *

Department of Applied Chemistry, National Chiao Tung University, Hsinchu, Taiwan 300, ROC

ARTICLE INFO

Article history:
Received 7 May 2013
Received in revised form
19 August 2013
Accepted 28 August 2013
Available online 4 September 2013

Keywords:
Colorimetric sensor
Al^{3+}
Gold nanoparticles
Triazole

ABSTRACT

A sensitive, selective colorimetric Al^{3+} detection method has been developed by using triazole–ether functionalized gold nanoparticles (TTP–AuNPs). Gold nanoparticles were prepared by reducing $HAuCl_4$ with sodium borohydride in the presence of 5-(1,2-dithiolan-3-yl)-*N*-(prop-2-yn-1-yl)pentanamide (TP). The azide part of 2-[2-(2-azidoethoxy)ethoxy]ethanol and the acetylene part of TP were combined to form a triazole structure through a click reaction. Aggregation of TTP–AuNPs was induced immediately in the presence of Al^{3+} ions, yielding a color change from red to blue. This Al^{3+}-induced aggregation of TTP–AuNPs was monitored first with the naked eye and then UV–vis spectroscopy with a detection limit of 18.0 nM. The TTP–AuNPs showed excellent selectivity for Al^{3+}, compared to other metal ions (Ag^{+}, Ca^{2+}, Cd^{2+}, Co^{2+}, Cu^{2+}, Cr^{3+}, Fe^{2+}, Fe^{3+}, Hg^{2+}, Mg^{2+}, Mn^{2+}, Ni^{2+}, Pb^{2+}, and Zn^{2+}). In addition, TTP–AuNPs were used to detect Al^{3+} in sea water samples, with low interference.

1. Introduction

Aluminum is the third most abundant element (after oxygen and silicon) and the most abundant metal element in the crust of the earth, accounting for about 8% of its mass [1,2]. Aluminum is widely used in our daily life, such as aluminum foil, vessels, and trays, therefore resulting in an increase of Al^{3+} concentration in food. According to a WHO report, the tolerable daily intake of aluminum is about 3 mg–10 mg and the acceptable weekly aluminum dietary intake in the human body is about 7 mg kg^{-1} of the body weight [3]. Excess Al^{3+} might change the structures of cells and damage cellular energy transfer processes and metabolism, resulting in cell death [4,5]. The cellular toxicity of aluminum has been connected to several diseases, such as Parkinson's disease (PD) [6], Alzheimer's disease (AD) [7], and dialysis encephalopathy [8].

Several methods for the detection of aluminum ions in various samples have been proposed [9], including atomic absorption spectrometry [10], and inductively coupled plasma mass spectroscopy (ICP-MS) [11], and voltammetry [12]. These methods either require the destruction of the sample, or are not easily employed in the case of assays. Recently, more attention has been focused on the development of selective and sensitive sensors for aluminum detection. Several fluorescent chemosensors for Al^{3+} detection have been reported [13–17]. Because they are made of organic molecules, they are not highly soluble in water and have higher detection limits. Colorimetric methods based on functionalized gold nanoparticles (AuNPs) are simple and convenient, and can solve these limitations.

Gold nanoparticles (AuNPs) show surface plasmon resonance (SPR) absorption properties, which are particularly sensitive to size, shape, and interparticle distance [18,19]. Many AuNPs-based colorimetric sensors use the interparticle plasmon coupling for analyte detection. In these assays, analyte-induced aggregation of AuNPs leads to a red shift in the SPR absorption band, resulting in a red-to-blue color change. On the other hand, the removal of analyte results in the redispersion of the aggregated AuNPs, causing the color to revert from blue to red. The distance-dependent SPR absorption of AuNPs has become a useful tool for the development of colorimetric sensing of various analytes, such as metal ions [20–30], anions [31–34], and oligonucleotides [35,36].

In this report, triazole–ether functionalized gold nanoparticles (TTP–AuNPs) were synthesized for detecting Al^{3+}. The gold nanoparticles were prepared through the borohydride-mediated reduction of $HAuCl_4$. 5-(1,2-Dithiolan-3-yl)–*N*-(prop-2-yn-1-yl) pentanamide (TP) was attached to the surface of AuNPs through the dithio group. Finally, the azide part of 2-([2-(2-azidoethoxy) ethoxy]ethanol and the acetylene part of TP were combined to form a triazole structure on the surface of AuNPs through a click reaction. The synthesized 5-(1,2-dithiolan-3-yl)–*N*-((1-(2-(2-(2-hydroxyethoxy) ethoxy)ethyl)-1H-1,2,3-triazol-4-yl)methyl)pentanamide AuNPs (TTP–AuNPs) can be used for metal ion detection (Scheme 1). Metal ions such as Ag^{+}, Al^{3+}, Ca^{2+}, Cd^{2+}, Co^{2+}, Cu^{2+}, Cr^{3+}, Fe^{2+}, Fe^{3+}, Hg^{2+}, Mg^{2+}, Mn^{2+}, Ni^{2+}, Pb^{2+}, and Zn^{2+} were

* Tel.: +886 3 5712121x56506.
E-mail addresses: spwu-mail@nctu.edu.tw, spwu@faculty.nctu.edu.tw (S.-P. Wu).

0039-9140/$ - see front matter © 2013 Elsevier B.V. All rights reserved.
http://dx.doi.org/10.1016/j.talanta.2013.08.054

tested for metal ion selectivity, but Al^{3+} was the only metal ion that caused the aggregation of TTP–AuNPs. This caused the SPR absorption band of TTP–AuNPs to shift to a longer wavelength, and consequently a color change from red to blue that in turn can be used to detect the presence of Al^{3+} ions. The SPR absorption at 700 nm directly indicated the degree of NTP-AuNP aggregation caused by the addition of Al^{3+} ions.

2. Experimental

2.1. Chemicals

Hydrogen tetrachloroaurate(III) tetrahydrate and $MgSO_4$ were obtained from Showa. Lipoic acid, *N*,*N*-diisopropylethylamine, $AgClO_4.\chi H_2O$ and $Pb(ClO_4)_2.3H_2O$ were purchased from Acros. Propargylamine, *O*-(benzotriazol-1-yl)-*N*,*N*,*N*′,*N*′-tetramethyluronium hexafluorophosphate (HBTU), sodium ascorbate, $Al(ClO_4)_3 \cdot 9H_2O$, and $Cr(ClO_4)_3 \cdot 6H_2O$ were obtained from Alfa Aesar. Sodium citrate tribasic dihydrate, sodium azide, $CuSO_4 \cdot 5H_2O$, $Ca(ClO_4)_2 \cdot 4H_2O$, $Cd(ClO_4)_2 \cdot xH_2O$, $CoCl_2 \cdot 6H_2O$, $Cu(BF_4)_2 \cdot xH_2O$, $Fe(BF_4)_2 \cdot 6H_2O$, $FeCl_3 \cdot 6H_2O$, $Hg(ClO_4)_2 \cdot xH_2O$, KBr, $Mg(ClO_4)_2 \cdot 6H_2O$, $Ni(O_2CCH_3) \cdot 4H_2O$, and $Zn(BF_4)_2 \cdot xH_2O$ were obtained from Sigma-Aldrich. $MnSO_4 \cdot H_2O$ was obtained from Riedel-de Haen. The transition metal ions were dissolved in the deionized water and stored at room temperature. For all aqueous solutions, deionized water (resistivity, 18.0 MΩ cm at 25 °C) purified by Millipore Direct-Q water purification unit was used. The synthesis procedure and characterization of 5-(1,2-dithiolan-3-yl)-*N*-(prop-2-yn-1-yl) pentanamide [37] and 2-(2-(2-azidoethoxy) ethoxy)ethanol [38] are described in the supporting information.

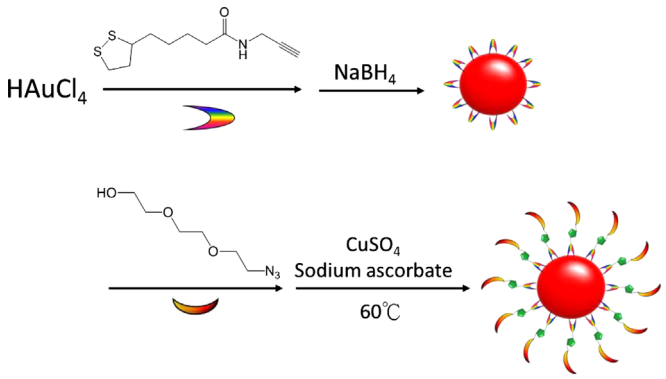

Scheme 1. Synthesis of TTP–AuNPs.

2.2. Instruments

UV–vis spectra were recorded on an Agilent 8453 UV–vis spectrometer (Santa Clara, CA, USA). IR data were obtained on Bomem DA8.3 Fourier-Transform Infrared Spectrometer (Quebec, Canada). TEM images were recorded from JEOL JEM-2010 Transmission Electron Microscope (Tokyo, Japan). ICP-MS data were recorded on an ICP-MS Perkin Elmer SCIEX ELAN 5000 (Waltham, MA, USA).

2.3. Preparation of TTP–AuNPs

Gold nanoparticles were prepared by reducing $HAuCl_4$ with sodium borohydride. All glassware was thoroughly cleaned with aqua regia (3:1 HCl/HNO_3) and rinsed with Millipore-Q water prior to use. Briefly, $HAuCl_4$ (80 mM, 270 μL) was added rapidly to a solution of 5-(1,2-dithiolan-3-yl)-*N*-(prop-2-yn-1-yl)pentanamide (0.01 M, 50 μL) that was stirred for further 15 min. Sodium borohydride (1 mL, 4 mg/mL) was slowly added to the mixture and stirred for 2 h. 2-(2-(2-Azidoethoxy)ethoxy)ethanol aqueous solution (0.01 M, 50 μL) was added into TP–AuNPs solution and stirred for 15 min. Finally, the mixture of copper sulfate (2 mM, 100 μL) and sodium ascorbate (20 mM, 100 μL) was added into TP–AuNPs solution and stirred for 3 h at 60 °C. The synthesized 5-(1,2-dithiolan-3-yl)-N-((1-(2-(2-(2-hydroxyethoxy)ethoxy)ethyl)-1H-1,2,3-triazol-4-yl)methyl) pentanamide-AuNPs (TTP–AuNPs) were dialyzed with 3.5 K MWCO Spectra/Por 7 membranes. The sizes of the TTP–AuNPs were verified by transmission electron microscope (TEM) analysis (Fig. 1).

2.4. Colorimetric detection of Al^{3+} ions

To a 1.0 mL of solution containing TTP–AuNPs, different metal ions ($[M^{n+}]=5$ μM) were added separately. The mixtures were maintained at room temperature for 10 min and then transferred separately into 1.5-mL quartz cuvette. Their SPR absorption bands were recorded by UV–vis spectrophotometer.

3. Results and discussion

3.1. Characterization of TTP–AuNPs

Gold nanoparticles were prepared through the borohydride-mediated reduction of $HAuCl_4$. 5-(1,2-Dithiolan-3-yl)-*N*-(prop-2-yn-1-yl)pentanamide (TP) was added into the AuNPs solution to be the capping agent. The azide part of 2-(2-(2-azidoethoxy) ethoxy)ethanol and the acetylene part of TP were combined to

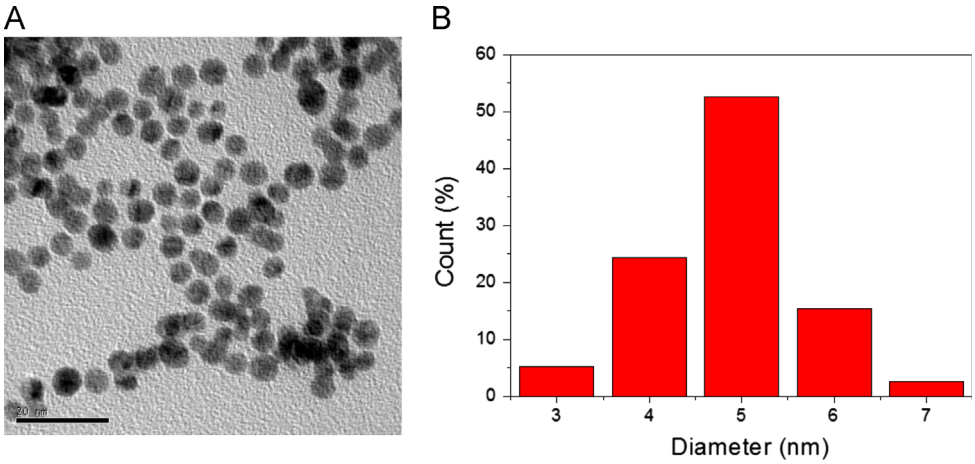

Fig. 1. (A) TEM image of TTP–AuNPs. The scale bar is 20 nm. (B) The size distribution of TTP–AuNPs.

form a triazole structure under the click reaction. The synthesized TTP–AuNPs can be used for further studies (Scheme 1). Transmission electron microscopy (TEM) image revealed that the particle size of TTP–AuNPs ranged from 3 nm to 7 nm, with most particle sizes falling in the range of 4 nm–5 nm (Fig. 1). The cycloaddition products from the click reaction were verified by infrared spectroscopy. As shown in Fig. 2a, the characteristic skeleton peaks of TTP–AuNPs were 3299 cm^{-1} (N–H), 2978 cm^{-1} (CH_2–0S), and 2118 cm^{-1} (–C≡CH). In Fig. 2b, the peak that was originally at 2118 cm^{-1} (–C≡CH) has disappeared, while new peaks at 2800 cm^{-1}–3500 cm^{-1} (O–H) have appeared, indicating that the click reaction has proceeded on the surface of AuNPs.

3.2. Interaction of TTP–AuNPs with various metal ions

To evaluate the selectivity of TTP–AuNPs towards various metal ions, the absorption spectra of TTP–AuNPs were taken in the presence of several metal ions: Ag^{+}, Al^{3+}, Ca^{2+}, Cd^{2+}, Co^{2+}, Cu^{2+}, Cr^{3+}, Fe^{2+}, Fe^{3+}, Hg^{2+}, Mg^{2+}, Mn^{2+}, Ni^{2+}, Pb^{2+}, and Zn^{2+}. Fig. 3 shows the effect of metal ions on the appearance of TTP–AuNPs in solution. Al^{3+} was the only ion that caused a SPR absorption peak to shift from 512 nm to 700 nm. This red shift was also observed as a color change from red to blue. Other metal ions did not influence the absorption spectra, indicating that no aggregation occurred. The triazole–ether units on TTP–AuNPs function as metal ion chelators. Al^{3+} binding between the triazole–ether units on TTP–AuNPs induced the aggregation of the TTP–AuNPs (Scheme 2). Fig. 4 shows the TEM image of the Al^{3+}-induced aggregation of TTP–AuNPs.

The degree of aggregation of TTP–AuNPs depended on the concentration of Al^{3+} ions; Fig. 5 shows the SPR absorption change with the addition of different concentrations of Al^{3+}. The absorbance at 512 nm decreased with increasing Al^{3+} concentration. The absorbance at 700 nm rose during Al^{3+} titration as a result of the Al^{3+}-induced aggregation of AuNPs. A linear relationship was found when the concentration of Al^{3+} ions was between 0.5 μM and 5 μM. The limit of detection for Al^{3+} was found to be 18.0 nM (see Figure S1 in supplementary data).

3.3. Interference studies

In order to study the influence of other metal ions on Al^{3+} binding to TTP–AuNPs, competitive experiments were carried out

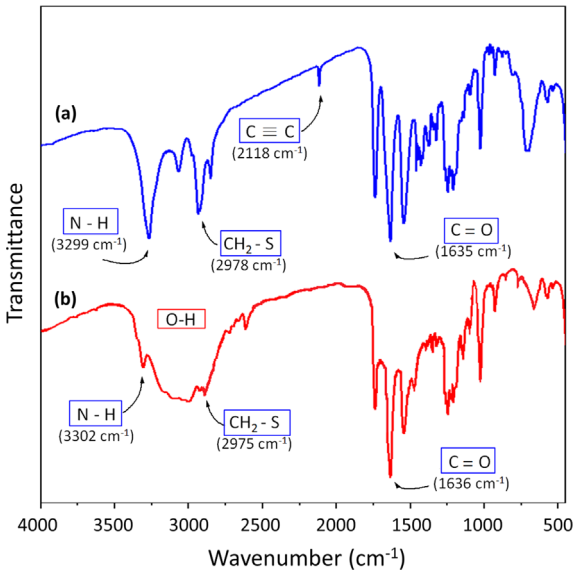

Fig. 2. FT-IR spectra of (a) TP–AuNPs and (b) TTP–AuNPs.

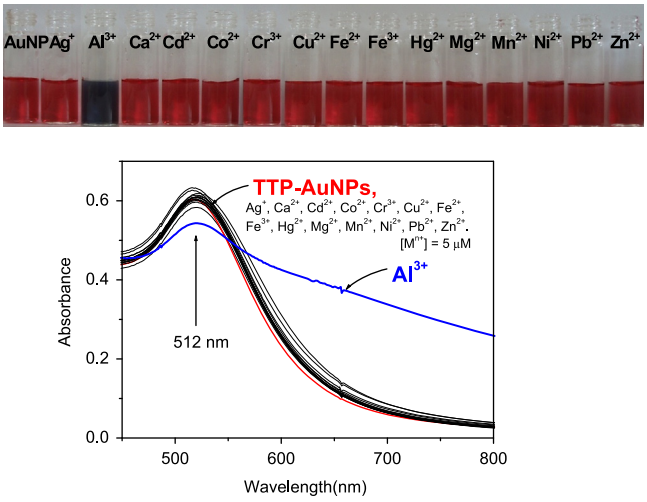

Fig. 3. (Top) Photographic images of TTP–AuNPs in the presence of various metal ions. (Bottom) UV–vis spectra of TTP–AuNPs in the presence of different metal ions (5 μM).

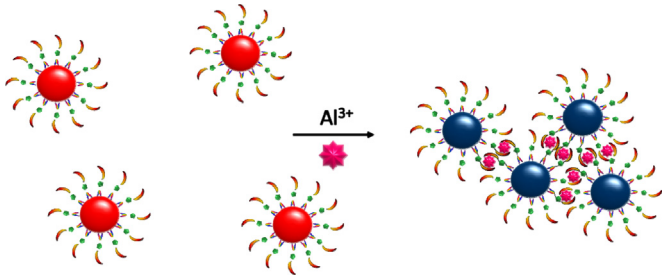

Scheme 2. Schematic depiction of the Al^{3+}-triggered aggregation of TTP–AuNPs for Al^{3+} detection.

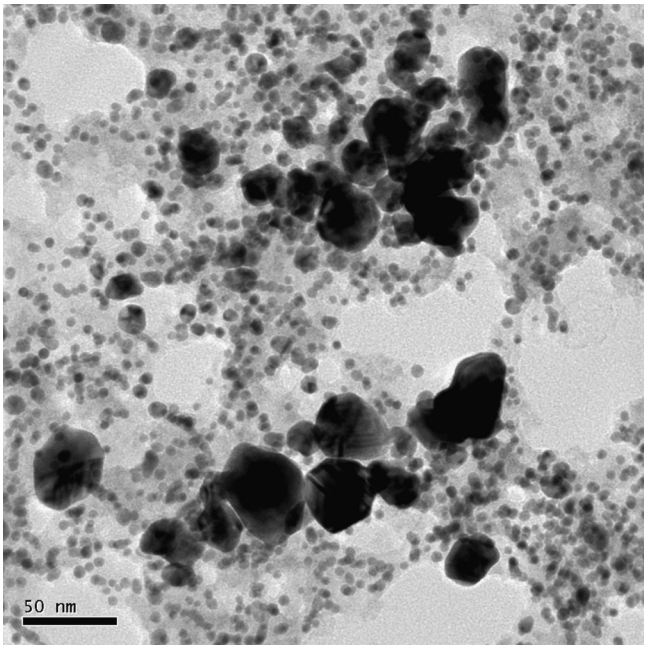

Fig. 4. TEM image of TTP–AuNPs in the presence of Al^{3+} ions (5 μM). The scale bar is 50 nm.

in the presence of Al^{3+} with Ag^{+}, Ca^{2+}, Cd^{2+}, Co^{2+}, Cu^{2+}, Cr^{3+}, Fe^{2+}, Fe^{3+}, Hg^{2+}, Mg^{2+}, Mn^{2+}, Ni^{2+}, Pb^{2+}, and Zn^{2+} (Fig. 6). The SPR absorption shift caused by the mixture of Al^{3+} with the other metal ion was similar to that caused solely by Al^{3+}. This indicates that other metal ions did not interfere in the binding of

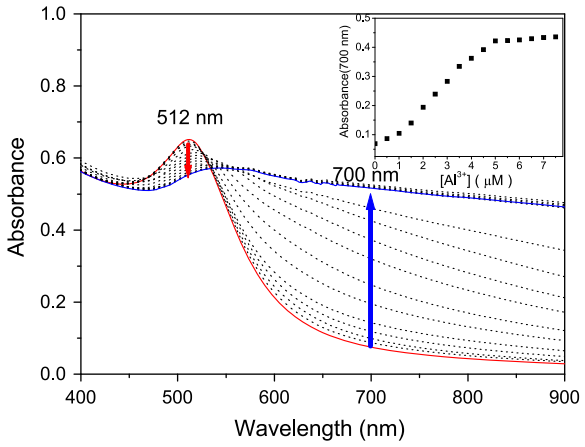

Fig. 5. Surface plasmon resonance absorption change of TTP–AuNPs in the presence of different concentrations of Al^{3+}.

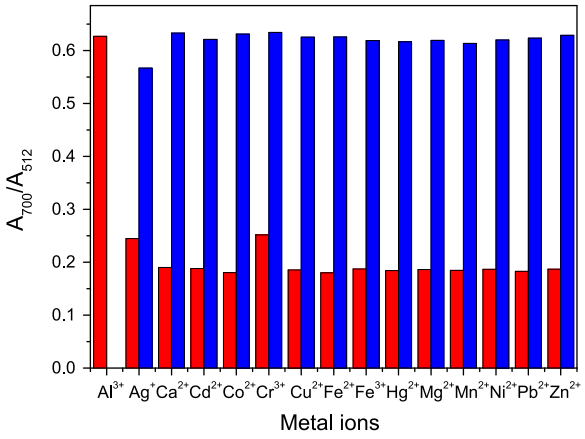

Fig. 6. Absorbance ratio ($A_{700\ nm}/A_{512\ nm}$) of TTP–AuNPs in the presence of metal ions. Red bars represent the addition of single metal ion (5 μM); blue bars are the mixture of Al^{3+} (5 μM) with another metal ion (5 μM). (For interpretation of the references to color in this figure, the reader is referred to the web version of this article).

TTP–AuNPs with Al^{3+}. This observation is consistent with previous studies suggesting that Al^{3+} is the only metal ion that can be bound to the TTP–AuNPs.

3.4. The influence of pH on Al^{3+}-induced aggregation of TTP–AuNPs

To investigate the suitable pH range in which TTP–AuNPs can effectively detect Al^{3+}, a pH titration of TTP–AuNPs was carried out. Fig. 7 shows that in the pH range of 3–10, the absorbance ratio (A_{700}/A_{512}) was constant. This indicates that TTP–AuNPs were stable in the pH range of 3–10. The influence of pH on Al^{3+}-induced aggregation of TTP–AuNPs is shown in Fig. 7; addition of Al^{3+} resulted in a high absorbance ratio (A_{700}/A_{512}) in a pH range of 3–6. At pH > 6, the absorbance ratio (A_{700}/A_{512}) decreased due to the formation of colloidal $Al(OH)_3$. These observations indicate that the pH range of 3–6 is suitable for monitoring Al^{3+} by TTP–AuNPs.

3.5. Application of TTP–AuNPs for the analysis of sea water samples

To test the practical application of TTP–AuNPs, sea water samples from the coastline located in Hsinchu, Taiwan were collected. All water samples were filtered through a 0.2 μm membrane and then spiked with different amounts of Al^{3+} standard solution. A calibration curve of TTP–AuNPs SPR that shifts in the presence of different concentrations of Al^{3+} was prepared (see Figure S2 in supplementary

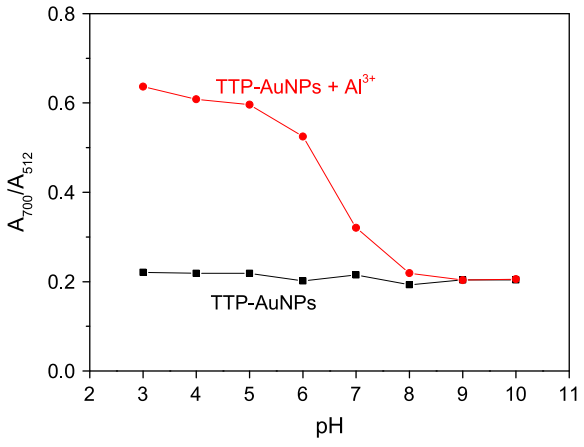

Fig. 7. Influence of pH on the UV–vis spectra of TTP–AuNPs in the absence and presence of Al^{3+} (5 μM).

Table 1
Results of Al^{3+} detection in sea water samples.

No	ICP-MS (M)	Proposed method[a]	Relative error(%)
sea water	5.33×10^{-8}	–[b]	–
sample 1	2.55×10^{-6}	$(2.43 \pm 0.04^{c}) \times 10^{-6}$ M	4.71
sample 2	3.66×10^{-6}	$(3.77 \pm 0.05^{c}) \times 10^{-6}$ M	3.01
sample 3	4.83×10^{-6}	$(4.67 \pm 0.05^{c}) \times 10^{-6}$ M	3.42

[a] by using TTP–AuNPs.
[b] Al^{3+} was not detected in sea water by TTP–AuNPs.
[c] Standard deviation with replicate number, 3.

data). The analytical results are shown in Table 1. The results obtained with TTP–AuNPs were in good agreement with those obtained using the ICP-MS method, with a relative error of less than 5%. These results demonstrate that the designed probe is applicable for Al^{3+} detection in sea water samples.

4. Conclusion

This report demonstrated that TTP–AuNPs can be used to effectively detect Al^{3+} ions. Al^{3+} was the only metal ion that induced aggregation of TTP–AuNPs, resulting in a color change from red to blue and a corresponding SPR absorption shift from 512 nm to 700 nm. The optimal pH range for Al^{3+} detection using TTP–AuNPs was determined to be from 3 to 6. In addition, TTP–AuNPs can be used to detect Al^{3+} in environmental samples.

Acknowledgments

We gratefully acknowledge the financial support of the National Science Council (ROC) and National Chiao Tung University.

Supplementary data

Synthesis of 5-(1,2-dithiolan-3-yl)-*N*-(prop-2-yn-1-yl)pentanamide and 2-(2-(2-azidoethoxy)ethoxy)ethanol, the calibration curve of TTP–AuNPs in water and the calibration curve for the detection of Al^{3+} by TTP–AuNPs.

Appendix A. Supplementary materials

Supplementary data associated with this article can be found in the online version at http://dx.doi.org/10.1016/j.talanta.2013.08.054.

References

[1] J.R. Walton, Encycl. Environmen. Health (2011) 331–342.
[2] J. Barcelo, C. Poschenrieder, Environ. Exp. Bot. 48 (2002) 75–92.
[3] Z. Krejpcio, R.W. Wójciak, Pol. J. Environ. Stud. 11 (2002) 251–254.
[4] M.A. Akeson, D.N. Munns, R.G. Burau, BBA-Biomembr. 986 (1989) 33–40.
[5] J.L. Greger, Annu. Rev. Nutr. 13 (1993) 43–63.
[6] E. Mendez-Aè Ivarez, R. Soto-Otero, A. Hermida-Ameijeiras, A.M. Lopez-Real, J.L. Labandeira-Garc, Biochim. Biophys. Acta. 1586 (2001) 155–168.
[7] K.P. Kepp, Chem. Rev. 112 (2012) 5193–5239.
[8] M.R. Wills, J. Savory, Lancet 322 (1983) 29–34.
[9] J. Tria, E.C.V. Butler, P.R. Haddad, A.R. Bowie, Anal. Chim. Acta. 731 (2012) 75–81.
[10] M. Frankowski, A. Zioła-Frankowska, J. Siepak, Talanta 80 (2010) 2120–2126.
[11] B. Chen, Y. Zeng, B. Hu, Talanta 81 (2010) 180–186.
[12] H. Wang, Z. Yu, Z. Wang, H. Hao, Y. Chen, P. Wan, Electroanalysis 23 (2011) 1095–1099.
[13] D. Maity, T. Govindaraju, Chem. Commun. 46 (2010) 4499–4501.
[14] C.R. Lohani, J. Kim, S. Chung, J. Yoon, K. Lee, Analyst 135 (2010) 2079–2084.
[15] L. Wang, W. Qin, X. Tang, W. Dou, W. Liu, Q. Teng, X. Yao, Org. Biomol. Chem. 8 (2010) 3751–3757.
[16] T. Han, X. Feng, B. Tong, J. Shi, L. Chen, J. Zhi, Y. Dong, Chem. Commun. 48 (2012) 416–418.
[17] Y. Liu, C. Chen, A. Wu, Analyst 137 (2012) 5201–5203.
[18] C. Burda, X. Chen, R. Narayanan, M.A. El-Sayed, Chem. Rev. 105 (2005) 1025–1102.
[19] M.-C. Daniel, D. Astruc, Chem. Rev. 104 (2004) 293–346.
[20] C.J. Murphy, A.M. Gole, S.E. Hunyadi, J.W. Stone, P.N. Sisco, A. Alkilany, B. E. Kinard, P. Hankins, Chem. Commun. (2008) 544–557.
[21] Z. Jiang, Y. Fan, M. Chen, A. Liang, X. Liao, G. Wen, X. Shen, X. He, H. Pan, H. Jiang, Anal. Chem. 81 (2009) 5439–5445.
[22] Y.Q. Dang, H.W. Li, B. Wang, L. Li, Y.Q. Wu, ACS Appl. Mater. Interfaces 1 (2009) 1533–1538.
[23] Y. Yao, D. Tian, H. Li, ACS Appl. Mater. Interfaces 2 (2010) 684–690.
[24] X. Li, J. Wang, L. Sun, Z. Wang, Chem. Commun. 46 (2010) 988–990.
[25] S. Wu, Y. Chen, Y. Sung, Analyst 136 (2011) 1887–1891.
[26] S. Chen, Y.M. Fang, Q. Xiao, J. Li, S.B. Li, H.J. Chen, J.J. Sun, H.H. Yang, Analyst 137 (2012) 2021–2023.
[27] L. Zhao, Y. Jin, Z. Yan, Y. Liu, H. Zhu, Anal. Chim. Acta 731 (2012) 75–81.
[28] S.K. Tripathy, J.Y. Woo, C.-S. Han, Sens. Actuators B 181 (2013) 114–118.
[29] R. Liu, Z. Chen, S Wang, C. Qu, L. Chen, Z. Wang, Talanta 112 (2013) 37–42.
[30] D. Tan, Y. He, X. Xing, Y. Zhao, H. Tang, D. Pang, Talanta 113 (2013) 26–30.
[31] K. Youk, K.M. Kim, A. Chatterjee, K.H. Ahn, Tetrahedron Lett. 49 (2008) 3652–3655.
[32] W.L. Daniel, M.S. Han, J.S. Lee, C.A. Mirkin, J. Am. Chem. Soc. 131 (2009) 6362–6363.
[33] L. Chen, W. Lu, X. Wang, L. Chen, Sens. Actuators B 182 (2013) 482–488.
[34] G. He, L. Zhao, K. Chen, Y. Liu, H. Zhu, Talanta 106 (2013) 73–78.
[35] C.A. Mirkin, R.L. Letsinger, R.C. Mucic, J.J. Storhoff, Nature 382 (1996) 607–609.
[36] H.X. Li, L. Rothberg, Proc. Natl. Acad. Sci. USA 101 (2004) 14036–14039.
[37] D. Garin, F. Oukhatar, A.B. Mahon, A.C. Try, M. Dubois-Dauphin, F.M. Laferia, M. Demeunynck, M.M. Sallanon, S. Chierici, Bioorg. Med. Chem. Lett. 21 (2011) 2203–2206.
[38] L.Q. Deng, O. Norberg, S. Uppalapati, M. Yan, O. Ramström, Org. Biomol. Chem. 9 (2011) 3188–3198.